Journal of Materials Chemistry C

Accepted Manuscript

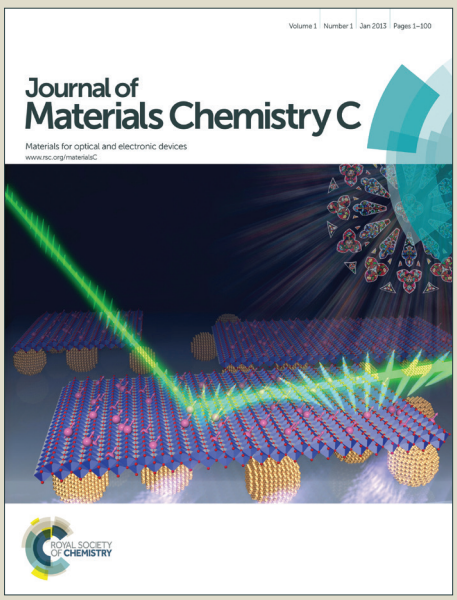

ROYAL SOCIETY OF CHEMISTRY

www.rsc.org/materialsC

Cite this: DOI: 10.1039/c0xx00000x

www.rsc.org/xxxxxx

ARTICLE TYPE

Particle tuning and modulation of the magnetic/colour synergy in Fe (II) spin crossover-polymer nanocomposites in a thermochromic sensor array

Alejandro Lapresta-Fernández,[a]* Manuel Pegalajar Cuéllar,[b] Juan Manuel Herrera,[c] Alfonso Salinas-Castillo,[a] María del Carmen Pegalajar,[b] Silvia Titos-Padilla,[c] Enrique Colacio[c] and Luis Fermín Capitán-Vallvey.[a]

Received (in XXX, XXX) Xth XXXXXXXXX 20XX, Accepted Xth XXXXXXXXX 20XX
DOI: 10.1039/b000000x

Thermochromic thin films of the spin crossover (SCO) polymer $[Fe(NH_2trz)_3](BF_4)$ are prepared using a variety of organic polymers as the host. The formation of different polymeric networks is confirmed macroscopically by the colour changes related to an SCO phenomenon induced by thermal variation, and the results are correlated with electron microscopy and energy dispersive X-ray spectroscopy. Large particles of the SCO material are observed in SCO/polymer hybrid systems with hydrophobic polymers, while more dispersed nano-crystals appear in the hydrophilic matrixes, leading to the transformation of the particles into fibrous structures. Subsequently, submicrometer-size SCO fibrous nanoparticles undergo colourimetric spin transitions near room temperature while grains with sizes larger than several microns move their transitions to lower temperatures. The difference in properties between the SCO/polymer hybrid materials is not only due to the differences in the size and shape of the SCO crystals in each polymer but also to the nature of the polymer and solvent interactions. The optical changes obtained for each SCO/polymer hybrid material are related to the microscopic origin of the cooperative interactions tracked by a photographic digital camera. A linear correlation is obtained (colour values versus temperature) when processing all the colourimetric data by artificial neural networks, thus avoiding the uncertainty inherent in the hysteresis loop.

Introduction

Applications of spin crossover (SCO) materials,[1] although attractive to develop, are still very scarce.[2,3] Their potential properties with the synergy shown between colour, magnetic moments and electrical resistance make them a valuable material for sensing technology.[4,5] Chemical temperature-sensing systems based on spin crossover materials are very poorly documented. Most of the room-temperature spin transition (ST) compounds are Fe(II) complexes derived from the 1,2,4-trz (trz = triazole) ligand system.[6] They are generally linear polymeric complexes $[Fe^{II}(4\text{-R-substituted-1,2,4-trz})_3]_n^{2n+}$ where the intersite interactions and thus the cooperative transition between a low-spin (LS) and a high-spin (HS) state are magnified.[7,8] This transition can be induced by thermal variation, and the spin-transition (abruptness, gradual, hysteresis or incomplete; note that no SCO chains with triazole are known to feature a double step transition) may confer a memory effect on the system when it exhibits hysteresis behaviour. The process is accompanied by colour changes from white (HS) to pink-violet (LS) near room temperature, also presenting thermal fluorescence variations when labelling SCO nanoparticles with an appropriate fluorophore like colloidal dispersions,[9] or when placed as thin films using soft lithography.[10] They offer the possibility of fine-tuning the thermally induced hysteresis loop, while the optical properties and the fluorophore remain unchanged. The thermochromic responses of these SCO materials are greater when compared with thermo-responsive polymers where the temperature change is fixed at set lower critical solution temperatures (LCST) such as 2-(2-methoxyethoxy)ethyl methacrylate (MEO_2MA)[11], poly(N-isopropylacrylamide) P(*N*-iPAAm) or with succinimide/isopropylasparamide segments.[12] On the other hand, depending on the nature of the surrounding environment, a matrix dependent cooperativity can be observed. It is well known that the metal-ligand distances in the metal coordination sphere directly reflect the spin state of the metal ion.[13] Generally, the LS state has a shorter metal-ligand (Fe-N) bond length than the HS, with the length changing between (0.14 – 0.24 Å).[6] In this respect, relatively weak ligands when coordinated to Fe(II) centres favour the HS state, generating weak coloured paramagnetic complexes. On the contrary, in case of strong ligands, the electrons maintain the spin paired configuration with S=0, obtaining an LS state and, often, coloured complexes.[14] Thus, the matrix environment is an important factor to modulate and/or transfer the SCO behaviour to novel functional materials in solid state, providing an opportunity to study the properties of these materials in polymers

or in unnatural environments such as biomembranes.[15-17] In a previous work developed by us, the linear SCO material, $[Fe(NH_2trz)_3](BF_4)_2$, was embedded in different polymeric matrices, forming thin films. There, the colour changes related to a spin crossover phenomenon induced by thermal variation offered a good correspondence with the magnetic measurements.[18]

Here, a colour/morphogenesis study is developed, providing a new outlook in the synthesis of SCO/polymer nanocomposites. Selecting polymers with different polarity, the polymeric microenvironment[19] where the $[Fe(NH_2trz)_3](BF_4)_2$ is embedded, can cause it to adopt different forms such as large aggregates or particles at the nanoscale. Depending on the nature of each polymer and the solvents used, different sizes of the SCO materials are produced. Thus, large aggregates of micrometer size (grains) are yielded in the presence of hydrophobic polymers, inducing a spin transition below room temperature that has ¡properties similar to the bulk material. On the other hand, submicrometer sized SCO particles were formed when using hydrophilic polymers, which involves a displacement of the spin transition to higher temperatures. Therefore, larger specific surface areas are produced when SCO nanoparticles are predominant, involving, presumably, higher interaction with the surrounding environment.[19] The SCO nanoparticles produce a pink colour (low state) at higher temperatures instead of a white colour in the case of micrometer particles. By using colourimetric measurements, then, the strength or weakness in terms of generating dense intermolecular interactions by solvent or polymer interactions with the SCO micrometer sized particles or with the SCO nanoparticles can be deduced. In all cases, the colour performance was directly related to the intrinsic features of the ST, determined optically.

If different colour changes appear for the same SCO material in each film, it might indicate that structural variations are occuring and so, by studying the intensity of these colour changes, a colour-structure correlation could be deduced. Thus, it is possible to design a colourimetric sensor array (CSA) of SCO materials[20-22] that can offer different colour changes when the SCO material is included in polymeric matrices of different polarity. The ST can be fine tuned by chemical modification of the material.[23,24] In this line, the synergy between the SCO phenomenon and the colour changes can be monitored using a photographic digital camera,[25,26] providing a simple method for sensing and imaging the temperature,[18] a possible alternative to traditional measurements.[27-29] Despite the fact that the hysteresis loop has associated uncertainty in the determination of temperature, successful temperature determination was accomplished with chemometric approaches involving an artificial neural network (ANN).

Results and discussion

First of all, it should be noted the magnetic susceptibility results and the thermochromic behaviour for the bulk SCO material synthesized as a powder and tracked by a photographic digital camera match quite well (see Figure 1). A correspondence was found for the green and a* channels from the RGB and CIEla*b* colour spaces, respectively, which confirms that the SCO transition can be optically tracked in this kind of system. The

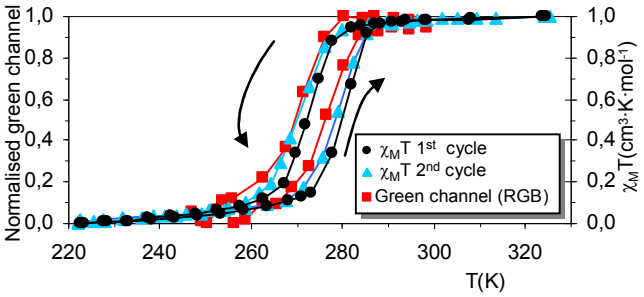

Figure 1. Correlation between the thermal variation in the colour intensity of $[Fe(NH_2trz)_3](BF_4)_2$ expressed as green channel values from RGB colour space and the thermal hysteresis of the χMT for $[Fe(NH_2trz)_3](BF_4)_2$.

optically detected hysteresis loop has a width of 6.9 K and is centred at ~ 273 K while the corresponding magnetic hysteresis loop has a width of 7.8 K and it is centred at ~ 276 K. (2^{nd} cycle green channel: ΔT: 5.0 K, centred at ~274 K; 2^{nd} $\chi_M T$ cycle: ΔT: 8.3 K, centred at ~ 274 K). In this regard, the value of $\chi_M T$ for the powder sample at 324 K is 3.5 $cm^3 \cdot K \cdot mol^{-1}$ which is consistent with the Fe(II) in the HS state (S=2). Figure 1 represents normalised values for both the colour and the magnetic measurements, making it possible to compare them properly. In the cooling mode, an abrupt SCO transition takes place, with the $\chi_M T$ reaching a value of 0.38 $cm^3 \cdot K \cdot mol^{-1}$ at ~222 K. Supporting the fact that the ST can be optically determined, Figure 2 shows a complete set of photographs between 248 and 323 K for six different SCO/polymer hybrid materials included in the CSA. The LS ↔ HS transition is easily observed as the colour changes simultaneously from one spin state to the other, and the thermochromic hysteresis loop can be detected for each series of photographs by the naked eye.

Identification and assignment of the structural features of the SCO/polymeric hybrid materials by microscopy

In order to obtain some insight into the morphology of the SCO particles once they are embedded within the organic polymers, scanning transmission electron microscopy (STEM) experiments were performed revealing that the SCO particles adopt different aggregation states depending on the polar nature of the polymers. In the presence of more hydrophobic polymers such as PVC, PS and PMMA, the SCO material has a strong tendency to form large clusters (grains) of individual SCO crystals (Figure 3.a, 3.e, S.2 and S.4), and spin transitions below room temperature are observed for the SCO/polymer hybrid materials. In all these cases, the cluster size is predominantly around 10 μm, but higher particle associations can also be found. Nevertheless, a tendency to decrease this dramatic aggregation is imaged for PMMA in THF, where the clusters are around 2-5 μm (Figure 3.i), while for PMMA in toluene single SCO, nanocrystals can be seen but high aggregation predominates (See Figure 3.h).

Looking at the slight differences in the size of the SCO material embedded in the hydrophobic polymers, with special focus on the lower population of single SCO nanocrystals, the minor differences in the colourimetric spin transition observed in Figure 6.1 for PMMA in toluene (small shift of the ST to higher temperatures, see also T½ data in Table 1) can be explained. Interestingly, additional structural differences between the thin

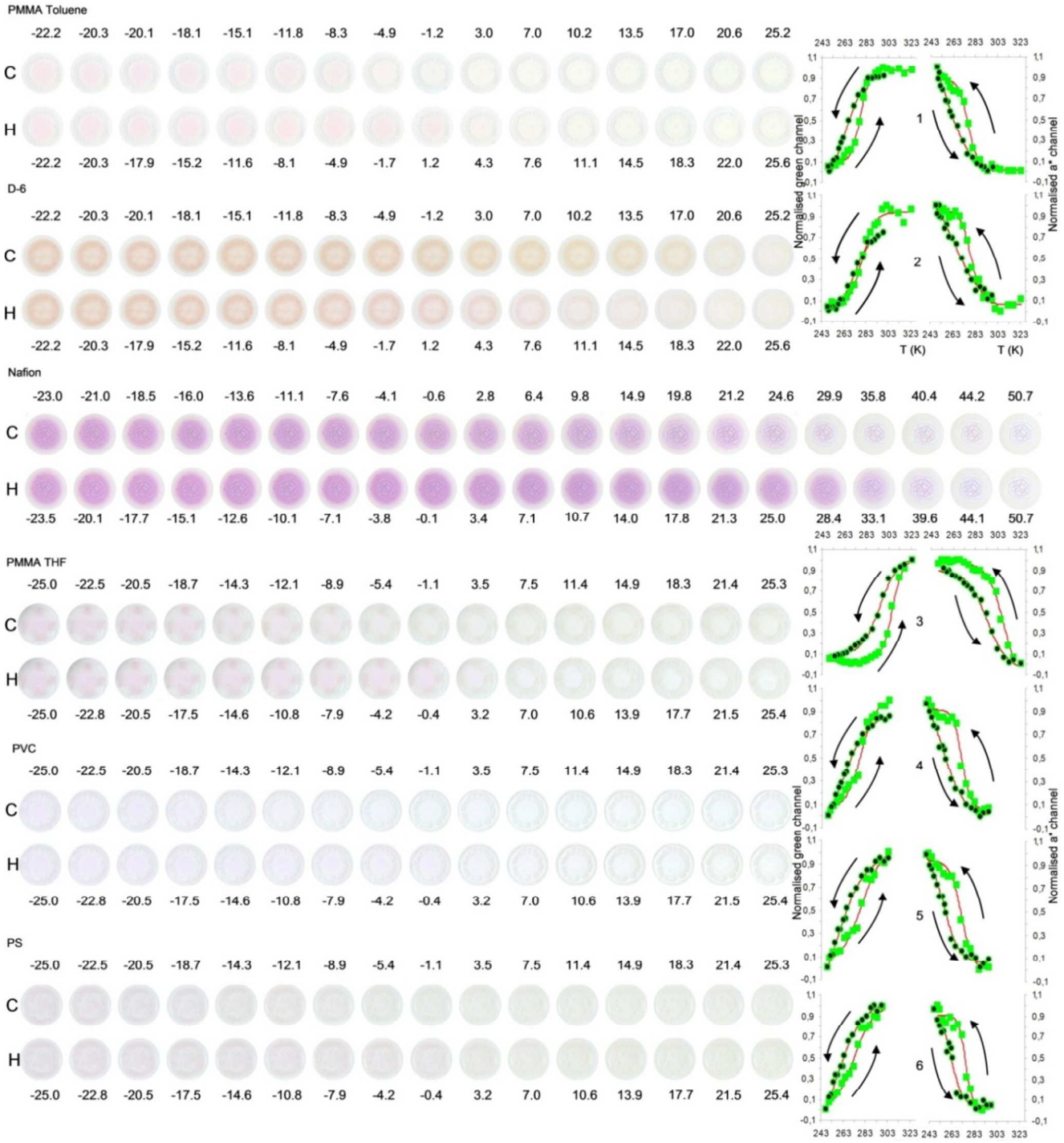

Figure 2. Photographed thermochromic behaviour of $[Fe(NH_2trz)_3](BF_4)_2$ in $PMMA_{toluene}$, D6, Nafion, $PMMA_{THF}$, PVC_{THF},PS_{THF} sensors. Colour fingerprints can be used for visual determination of temperature ranges. Colour changes related to the hysteresis loop can be observed for each series of sensors. (1) left: corresponds to green colour coordinate variation induced by temperature changes (1) right corresponds to a* colour coordinate variation induced by temperature changes. Both are for SCO/$PMMA_{toluene}$ sensors. The same parameters are placed in (2), (3), (4), (5) and (6) for D6, Nafion, $PMMA_{THF}$, PVC_{THF} and PS_{THF} sensors, respectively. Numbers inside correspond to degree Celsius (°C).

films can be found when different polarity solvents are used.

For THF, a more porous polymeric thin film is observed (see Figure 3.b, 3.e, 3.i and 3.j) while a more continuous film appears with toluene (Figure 3.h). Therefore, not only can the nature of the solvent affect the spin transition,[30] but also the different structure of the polymers covering the SCO material, as is seen to occur in the colourimetric ST using PMMA with toluene and THF (see Figure 6.1). On the other hand, when using hydrophilic polymers such as Nafion and polyurethane D6, fibre-shaped SCO nanoparticles can be imaged, which induces an abrupt change in the colour properties. In these cases, due to the decrease in the SCO material size, larger specific surface areas are involved in the network system, which can develop higher interactions with the surrounding chemical environment.

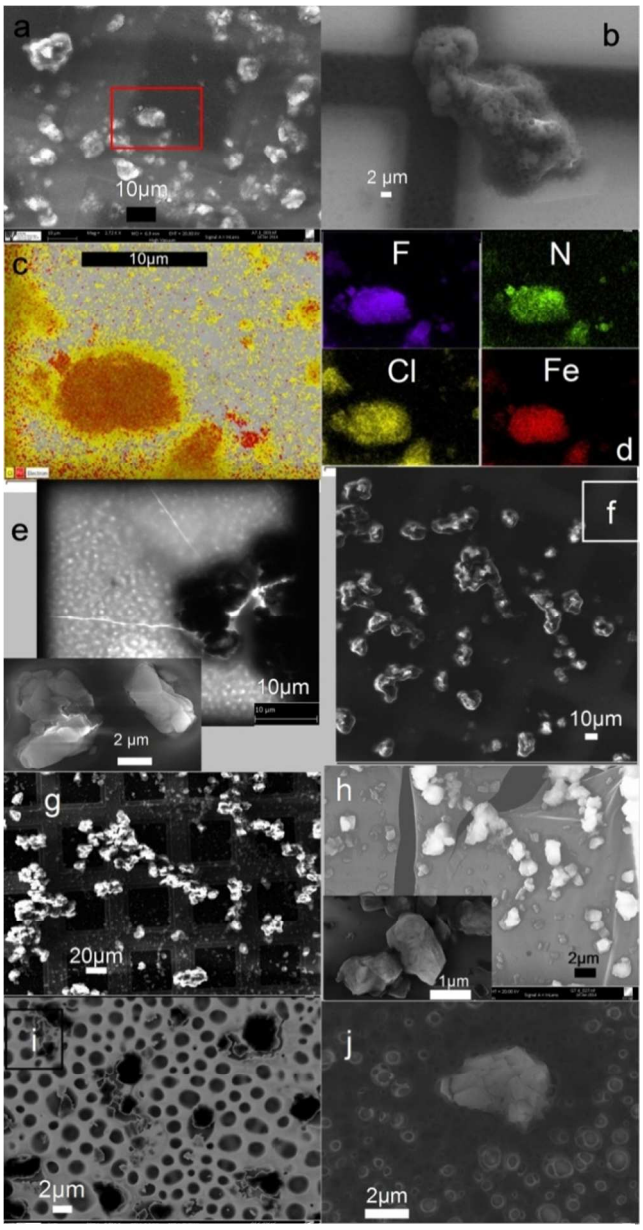

Figure 3. STEM images of the SCO material immobilized in different polymers (a) in PVC, (b) Imaging of a cluster surrounded by a porogeneus film of PVC, (c) Energy-dispersive X-ray spectroscopy for Fe (red) and Cl (yellow); the SCO/polymer hybrid material is seen as an overlapping orange colour, (d) EDX element mapping of F, N, Cl and Fe. (e) in PS 10 μm clusters are also found. The inset is magnified cluster morphology since they are composed of individual SCO particles. (f) Representative image of SCO/PS hybrid materials. (g) Representative image of SCO/PMMA in toluene as clusters of 10 μm, (h) submicrometer SCO particles reveal that some of them are dispersed and the inset is a magnification. (i) SCO/PMMA in THF between 2 and 5 μm-size and porous in the thin film, (j) Image of one cluster where the aggregation of SCO particles and the porosity of the thin film are clearly seen.

A microelemental analysis of the SCO/polymer hybrid material was carried out by EDX.[31] Thus, a qualitative view of the elemental composition in the inspection area is obtained when rastering over a relatively large inspection field (see Figure 3.c and d). The EDX element mapping was obtained for the SCO material immobilized in PVC since this polymer has an element (Cl) which is different from the element composition of the SCO material. As expected, EDX analysis reveals the presence of the Fe-trz polymer (F, N, Fe elements) embedded within a uniform shell of polymer (Cl element) (see Figure 3.c and d). See also Figure S.3 for more details. An EDX analysis for the other SCO hybrid materials with hydrophobic polymers was carried out on a specific localization instead of doing an elemental mapping. In all cases, the results of the EDX analysis agree with the nature of each SCO/polymer hybrid material (see Figures S.5, S.6 and S.7).

In the presence of hydrophilic polymers, such as Nafion and polyurethane D6, the SCO material develops larger differences in structure and morphology than in the presence of hydrophilic polymers. To investigate the morphology changes in detail we first observed what happens macroscopically and after that, we further characterized them by STEM and SEM.

Figure 4.a shows that the SCO material in D6 and Nafion becomes a pink-violet gelatinous material, while in the hydrophobic cocktails it retains the appearance of the net SCO material (white powder), which indicates an apparent change in its structure. The gel formation is irreversible, which is not typical for physical gels.[30] According to the data discussed above, it seems that these changes can depend on the SCO particle morphology (size and shape) as well as on possible interactions with the chemical environment. Clearly, the size and shape of the SCO particles underwent substantial changes during the cocktail homogenization (from Figure 4.b, until 4.g for the SCO in Nafion and from Figure 4.i to 4.l in D6). The SCO particles (See Figure S.1), when synthesized as a bulk, are predominantly formed by large clusters of ~500 nm with a low population of ~1 micron particles. However, in the SCO/polymer hybrid materials, the SCO are formed by a low population of ~10 μm clusters and a large population of sticks, needles and fibres reaching several hundred nm and microns. Therefore, the change in the SCO properties can be related to the evolution of the material morphology and/or to the removal of residual solvent molecules during the controlled evaporation to form the thin film. It is well known that the non-coordinated solvent molecules in most triazole-based Fe(II) SCO complexes influence the interlinking of the SCO centres, producing different transition temperatures.[27]

Like the case of PVC, EDX element mapping was performed for the SCO material immobilized in Nafion since that polymer has an element (S) different from the element composition of the SCO material. The formation of the SCO/polymer hybrid material is further demonstrated by the element mapping of F, C, Fe and S, revealing the Fe of the SCO material, S from the Nafion polymeric film and F and C, which can be associated with both the SCO material and the Nafion as the individual element maps confirm in Figure 4.h. Figures S.10, S.11 and S.12 are field enlargements of Figures 4.b 4.f and 4.i to better observe the size and morphology of the clusters and fibre-like particles in Nafion.

In the case of polyurethane D6, the obtained gel corresponds microscopically to a small cluster population around 10 μm (and larger) with a predominant morphology based on needle-shaped structures several micrometers in length and varying from 250-500 nm in width. (Figure 4.i, 4.j and 4.l for fibre-like structures and Fig 4.k shows a cluster). Microelemental analysis for the SCO/D6 hybrid material can be seen in Figure S.9. When using Nafion, a less homogeneous material predominantly composed of shorter particles and fibres than in D6 is obtained (see Figure 4.b

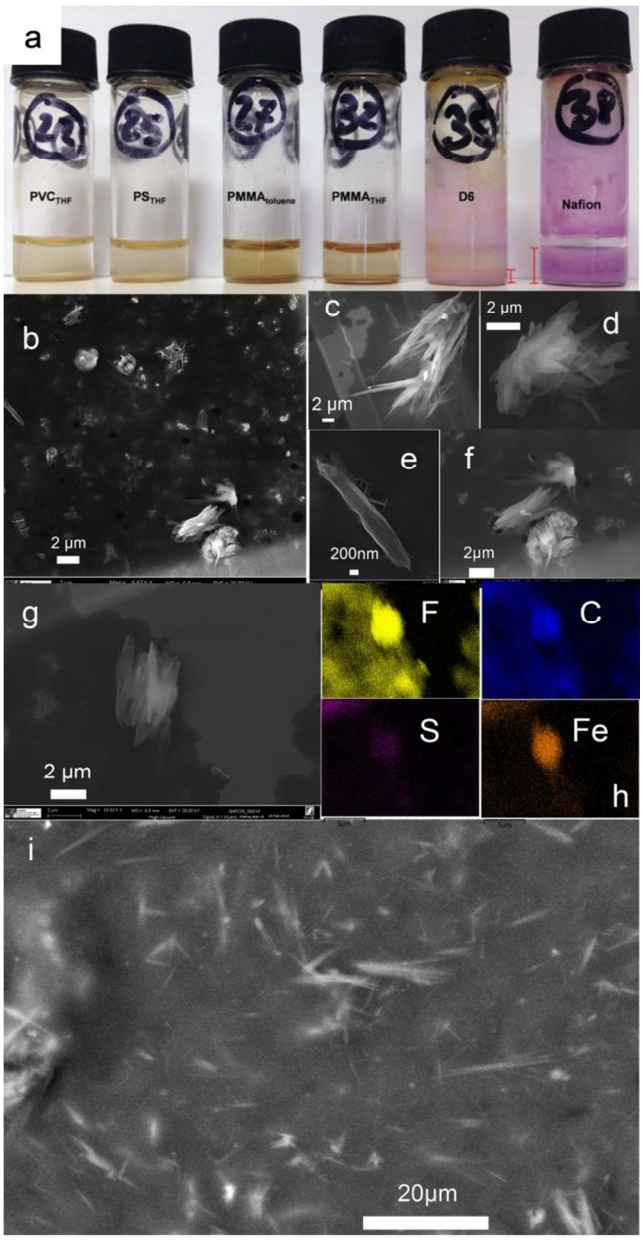

Figure 4. (a) Cocktails containing the same amount of SCO material. Gel formation is only observed for D6 and Nafion as well as a colour change from white to pink-violet. (b) Representative image of the SCO/Nafion hybrid material. Cluster around 5 µm, smaller associations of 1 µm as well as short fibres about 2 µm are observed. (c), (d) and (f) represent images of 5 µm cluster. (e) Magnification of short fibre around 2 µm (g) Image of 5 a cluster of 5 µm used for the Energy-dispersive X-ray spectroscopy analysis. Aggregation of short fibres can be observed. EDX element mapping of F, C,S and Fe. (i) Representative image of the larger fibres observed for the SCO/D6 hybrid material.

to 4.g). It is most likely that the Nafion composition and its dissolution in a mixture of solvents, such as aliphatic alcohols and water, lead to a redistribution of the fibrous architectures.

Although the presence of F can also be attributed to Nafion, the localization of S in the element map in Figure 4.h is due exclusively to the Nafion, which indicates the presence of the polymer coating in a thin film. Therefore, when using hydrophilic polymers, the change in the chemical composition and the use of different solvents have a marked influence on both the particle aggregation and the solution processes involving different evolutions of the SCO particle morphology, which ultimately develops different SCO properties and transition temperatures (see Figure 6).

Considering these results, it is possible to find close connections between the colour information and the changes in the crystalline network (nanoparticles, fibres and grains of several microns) of the SCO material. Here, larger clusters of the SCO material were observed in the hydrophobic polymer while more dispersed nanoparticles appeared in the hydrophilic matrix. The differences found in the SCO particle size and morphology for the distinct SCO/polymer hybrid materials produce a different ST, which in turn produces the colour changes related to the thermal induced spin crossover phenomenon.

Polymer influence on the SCO phenomenon by colour measurements

With regards to the colour variations between the HS and the LS, it is possible to determine which polymer exhibits more influence on the SCO material. Only the green channel in the RGB system and the a* colour coordinate from the CIEL*a*b*L* correlate well since they preserve the largest difference in histogram values for all the sensors studied and offer a better correspondence between the experimental data. Both, the green and the a* experimental values follow an ST curve with hysteresis. (See Figure 2). However, the ST for all the thin layers of the colourimetric sensor array (CSA) is generally less abrupt than that observed for the bulk and the square shape of the hysteresis is lost. This behaviour was observed by Cobo et al[20] and can be attributed, as in our case, to solvent effects. Moreover, it is known that with this kind of SCO system, the magnetic behaviour is strongly influenced by the presence of organic polymers or surfactant molecules embedding the materials due to the existence of supramolecular interactions between these coating agents and the SCO particles.[19,32] The physical parameters characteristic of the SCO transition, considering the colour differences (green channel value) are listed in Table 1. According to these data, it is clear that the different types of polymers affect the LS ↔ HS transition in a very different way. Both colours, white (paramagnetic- high temperatures, HS) and pink-violet (diamagnetic- low temperature, LS), reflect the strength of the interactions between the spin centres in each thin film.[33]

In this respect, the larger the colour differences, the stronger the influence between the polymers and the Fe-trz chains (see Figure 5). Therefore, the following trend can be established:

Nafion > D6 > PMMA$_{toluene}$ > PMMA$_{THF}$ > PVC$_{THF}$ ~ PS$_{THF}$

where the Nafion exhibits the strongest influence while the PVC$_{THF}$ and the PS$_{THF}$ hybrid materials present the weakest influence on the Fe-trz chains, following the same trend observed for the polar nature of the polymers (from hydrophilic to hydrophobic). Taking into account these colourimetric data, it also seems that the degree of interaction between the hydrophobic polymers and the Fe-trz particles is rather weak (inducing weak colours), favouring the HS state, which displays properties similar to the bulk material. Conversely, as the hydrophilic nature of the polymer increases, the degree of interaction is stronger and

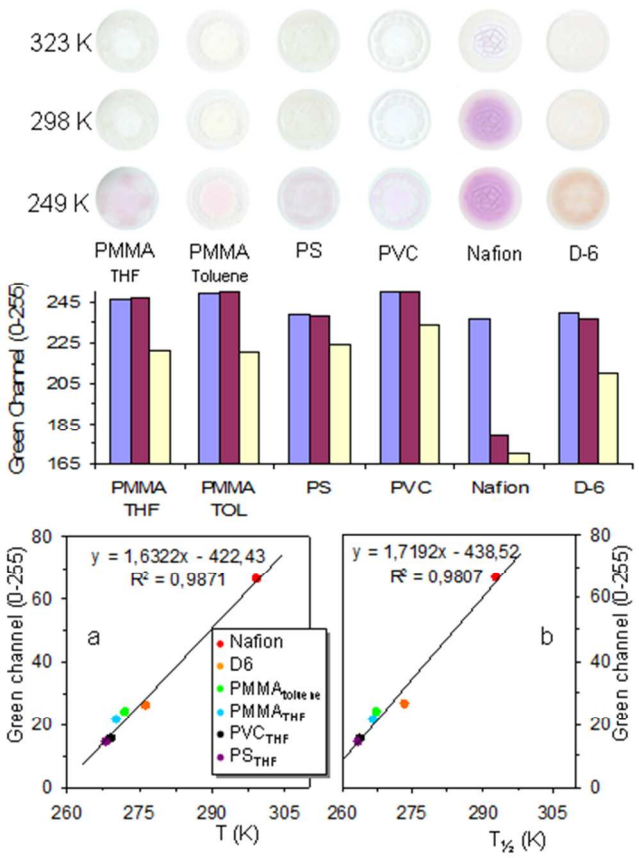

Figure 5. SCO/polymeric hybrid materials related to colour changes at 323, 298 and 249 K which correspond to blue, purple and yellow, respectively. Differences in green channel values between the white (highest temperature) and pink/violet (lowest temperature) for each tested sensor: $PMMA_{toluene}$: 28.6; $PMMA_{THF}$: 24.2; Nafion: 67.2; D6: 29.4; PVC_{THF}: 16.4 and PS_{THF}: 15.1. Relationship between the green value differences from RGB and (a) $T_{½}$ (↓), and (b) the midpoint temperatures of the hysteresis ST.

the LS state is favoured (inducing strong colours). An optically size-property correlation can thus be established. The above trend is supported by the $T_{½}$ (↓) values and by the Figure 6.2.

A linear relationship between the green channel of RGB with the midpoint temperatures of the hysteresis ST (Figure 5b) and the temperature in cooling mode, $T_{½}$ (↓), (Figure 5a) can be established, thus supporting the above colour trend. Observing the data in Table 1, SCO/Nafion shows the highest $T_{½}$ (↓) at 292.9 K with the other hybrid materials following the previously established trend, from 273.3 K to 263.5 K for D6 and Ps_{THF}, respectively. This is also true for the midpoint temperatures of the transitions, i.e. the hysteresis centre, suggesting that a relationship between the observed colour and the hysteresis parameters exists for the SCO/polymer hybrid material forming the CSA.

Solvent effect

As indicated above, the SCO properties of the Fe-trz family of complexes is strongly influenced by the existence of solvents or surfactant molecules within the crystalline network.[6,30] Here, this effect is demonstrated with colourimetric measurements. In our case, solvents with different dielectric constants ranging from polar protic (ethanol, water) to polar aprotic (THF) or non-polar (toluene) were used and significant changes to the SCO parameters were observed. For example, whereas the SCO/PMMA hybrid material prepared with toluene exhibits a complete spin transition closer to a square-shaped hysteresis loop of 9.2 K in width, with the prepared material forming highly polar THF, the transition is not complete and the hysteresis width is reduced to 7.0 K. Figure 6.1 demonstrates the improvement in the ST characteristics, i.e. in the square shape of the hysteresis, following a decrease in the solvent polarity to a dehydrated powder.

Table 1. Spin crossover process data of the SCO/polymer hybrid material

material	Colour differences	$T_{½}$(↓) (K)	$\Delta T_{½}$ (K)	Hysteresis loop (K)	hysteresis centre (K)[b]
Powder $\chi_M T$ 1st cycle	-	271.9(↓)	7.8	259-292	275.8
Powder $\chi_M T$ 2nd cycle	-	270.0(↓)	8.3	253-295	274.2
Green channel from RGB[a]					
Powder 1st cycle	24.3	269.3(↓)	6.9	253-292	272.8
Powder 2nd cycle	21.6	271.9(↓)	5.0	260-290	274.4
SCO/polymer[a]					
Nafion	66.2	292.9(↓)	12.6	248-323	299.2
D6	26.3	273.3(↓)	6.5	258-282	276.5
$PMMA_{toluene}$	24.1	267.5(↓)	9.2	253-286	272.1
$PMMA_{THF}$	21.5	266.8(↓)	7.0	251-281	270.3
PVC_{THF}	15.2	263.9(↓)	10.6	250-293	269.2
PS_{THF}	14.3	263.5(↓)	9.5	249-298	268.2

Experimental green channel values were adjusted to a sigmoidal fit using a Boltzmann type equation. [a]Data obtained from green channel values. [b] Arithmetic mean from T½(↓) and T½ (↑) . ΔT½: hysteresis width

Interaction network

It is particularly notable that a wide hysteresis loop was only found in the case of the SCO/Nafion hybrid material where the experimental spin transition between the LS (S = 0, pink-purple colour) and the HS (S = 2, white colour) takes place between 248 and 323 K (~ 30 K higher than with the other hybrid materials), with a width of 12.6 K (the largest value of all of them) and centred around 299 K (the most shifted to higher temperatures) (see table 1). This ST is shifted ~30 K to a higher temperature with respect to that observed for the susceptibility measurements in the powder sample, while the other polymers show more similar spin transition centres. A possible explanation of this intriguing behaviour lies in the Nafion structure when it forms thin films. According to the suggested model of parallel cylindrical water nanochannels for Nafion,[34] long parallel packed water channels (2.4 nm average diameter) are surrounded by partially hydrophilic side branches, forming inverted-micelle

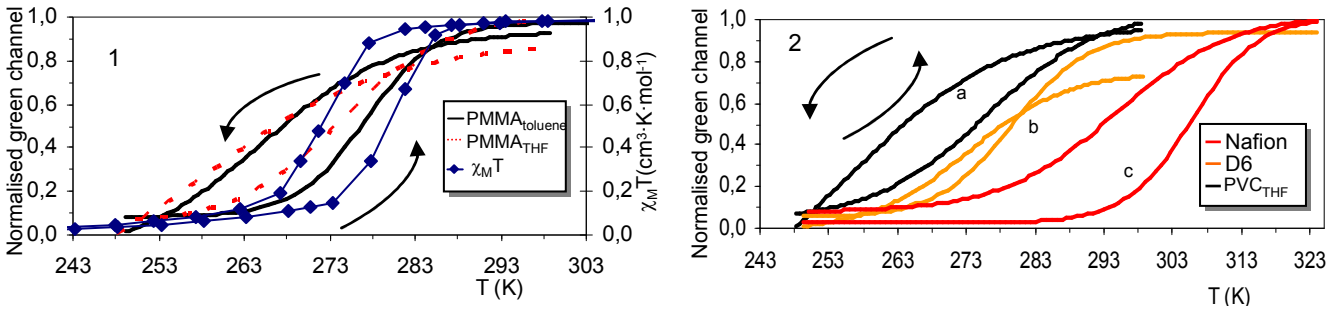

Figure 6. (1) Effect on the green channel values of the presence of a non-polar solvent (Toluene) and a polar aprotic solvent (THF) regarding SCO/PMMA sensors. Dashed line: $PMMA_{THF}$. Continuous line: $PMMA_{toluene}$. (2) Displacement of the ST to higher temperatures due to (1) the presence of water molecules, polar solvent (ethanol) (2) the nature of the polymer and (3) morphology of the SCO crystals, all generating different interactions of the crystal lattice. Strength sequence based on the observed colour: (c) Nafion, >(b) D6 and > (a) PVC_{THF}.

cylinders. Here, Nafion crystallites (~10 vol%) are forming physical crosslinks, elongated and parallel to the water channels that are crucial for the mechanical properties of Nafion films. Thus, hydrophilic groups such as $-SO_3^-$ (coming from the end groups linked in perfluoroalkylether polymeric chains of Nafion)[35] Fe(II) ions, nitrogen of triazole and the counterions BF_4^- are located inside these cylinders forming self-assembling magnetically and optically active nanoscale networks.[35,36] It is known that the $[Fe(NH_2trz)_3]$ chains of 1-D polymeric nature in the crystal structure, apart from showing interactions with the BF_4^- anions, exhibit intermolecular interactions through hydrogen bonding with the water molecules,[33,37] and $R\text{-}SO_3^-$ is acceptable as a counter anion.[35]

All the SO_3^- groups and the water molecules can participate in the crystal cohesion of the SCO complex, producing these interactions in the water channel. In this respect, a structural change is achieved with Nafion by increasing the density of the intermolecular interactions,[33] leading to a shortening of the Fe-N distance that corresponds to the LS distances (1.96–2.00 Å),[6,37] and in turn, producing a purple colour. This seems to indicate that the LS form is thermodynamically more favoured at room temperature (298 K). These more dense interchain interaction networks, together with the different size and shape of the SCO material, might explain why the SCO-Nafion hybrid material exhibits a purple colour at room temperature while the powder sample of the bulk material is white, showing a wide ST. Thus, three types of effects could make the spin transition produce a large thermal hysteresis loop: (1) morphology of the SCO crystals (2) the presence of solvent (water and aliphatic alcohols) molecules inducing strong interactions, with LS prevailing over HS at room temperature and (3) the presence of Nafion crystals, according to the accepted model.[34] These facts are supported by observing the behaviour of the SCO material in D6 (the other hydrophilic polymer tested). In the SCO/D-6 film, a light brown colour is visually observed around room temperature. This colour could indicate, as in the case of the SCO/Nafion hybrid material, that the LS for the SCO/D-6 film is also more favoured at room temperature than the HS (in powder the most favoured thermodynamical state at room temperature corresponds to HS, the white colour). Therefore, more dense interactions are being produced in the SCO crystals, which can be attributed to the presence of water molecules and polar solvents (D6 is mixed with water and ethanol 9:1), as well as to the larger specific surface area of the SCO fibres, allowing a better interaction with the chemical environment. Moreover, the hysteresis loop in D6 is narrower (from 258 to 282 K and similar to other cases) than that observed for the SCO/Nafion material (248 to 323 K). Since both Nafion and D6 polymers were dissolved in a similar alcoholic mixture and both present similar SCO fibres, the wide hysteresis loop for the SCO/Nafion hybrid material could be attributed to the presence of the Nafion crystallites, which are crucial for the outstanding properties of Nafion in the model described above.

Memory effect

As the ST parameters may depend on the number of temperature cycles, five complete temperature cycles were monitored for each SCO/polymeric hybrid material by a digital photographic camera. With the SCO/polymer hybrid materials that exhibit less intense colours in the CSA, i.e. with $PMMA_{THF}$, PVC_{THF} and PS_{THF}, the hysteresis centre was progressively displaced to higher temperatures along the cycles to reach values of 273.4 K, 271.9 K and 270.6 K, respectively. With regard to the hybrid materials

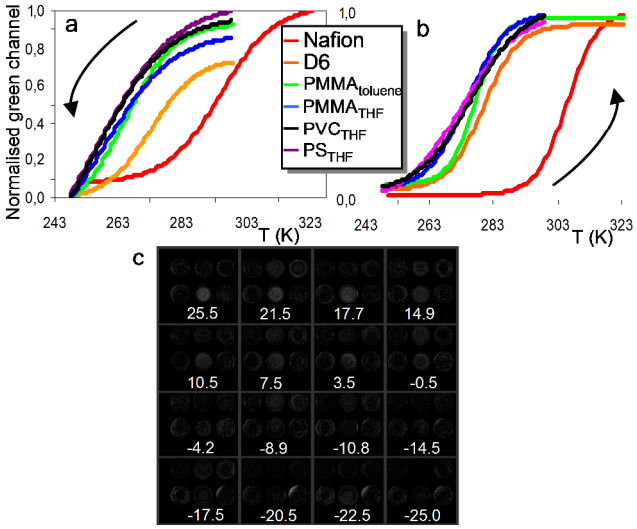

Figure 7. Effect on the ST shape. These materials display an abrupt ST in the heating mode (b) while a smoother transition is shown when cooling (a). The lines correspond to the Boltzmann fit of the experimental green values from RGB. (c) Difference maps of the colour offered by the CSA in cooling and heating modes. Numbers inside correspond to degree Celsius (°C). Film positions: First row: PS_{THF}; D6 and $PMMA_{toluene}$. Second row: PVC_{THF}; Nafion and $PMMA_{THF}$.

that offer more intense colours, SCO/Nafion gives practically the same position of the hysteresis centre at around 297.9 K, also maintaining a similar ST shape. For $PMMA_{toluene}$ and D6, the $T_{½}(\uparrow)$ remains almost constant at around 278.0 K and 279.9 K respectively, while $T_{½}(\downarrow)$ is progressively shifted toward higher temperatures, ~ 4 K each , to reach values of 268.9 K and 277.8 K over the cycles, respectively. In both cases the hysteresis width ($\Delta T_{½}$) decreased several K, ranging from 6.5 to 2.5 K for D6 and from 12.3 to 9.1 K in case of PMMA in toluene. In the latter case, a loss of sensitivity in the ~ 298 and 248 K temperature range occurs during the cycle sequence as previously reported.[18]

This loss of sensitivity is observed for all SCO/polymeric hybrid materials, except for D6. Interestingly, a more abrupt tendency was found during heating than in the cooling mode, which results in a more gradual spin-crossover (See Figure 7).

As indicated above, the transition for the SCO/D6 hybrid material occurs with a relatively narrow thermal hysteresis loop over the 263 - 297 K temperature range. From the cycle-by-cycle trend, the hysteresis width remained constant for the 3rd and 4th cycle with a reproducible hysteresis loop with a short width of 2.5 K. This fact was previously used to design an optical sensor, decreasing the uncertainty in the hysteresis loop from ~ 263 to 297 K.[18]

CSA visual fingerprint

The printed arrays were tested extensively against five temperature cycles and digitally imaged using a conventional photographic digital camera. Each SCO/hybrid material changes its colour after a few seconds of exposure, yielding a unique colour fingerprint for each specific temperature. Figure 8 shows that it is possible to differentiate whether a cooling or heating process has taken place in the CSA, since different colours are related to the different cooling or heating modes. Inverted colours are also displayed in Figure 8 since they improve a visual discrimination between each CSA. All data analysis, however, relies strictly on the original digital differences in the green channel from RGB values, as in Suslick et al.,[38-40] with the inverted colour shown only to help naked eye visualization. Figure 8 also shows how the SCO/polymer hybrid materials with both higher midpoint temperatures of the hysteresis and $T_{½}(\downarrow)$ start to change their colour at high temperatures while the other hybrid materials contribute, gradually, to the visual fingerprint when the temperature decreases. Therefore, a rapid temperature determination can be accomplished by the CSA easily by the naked eye where the CSA response to each temperature is represented by a unique pattern. Figure 7.c. shows the differences in the colour arrays between cooling and heating modes, visually indicating the presence of the thermal hysteresis loop. Although these differences help to know whether a certain temperature was reached by cooling or heating, it confers a memory effect on the system which inherently increases the uncertainty of the temperature quantification. However, one advantage of array-based chemical sensing is that all the responses can be combined to design a sensor that resolves this uncertainty, as discussed below.

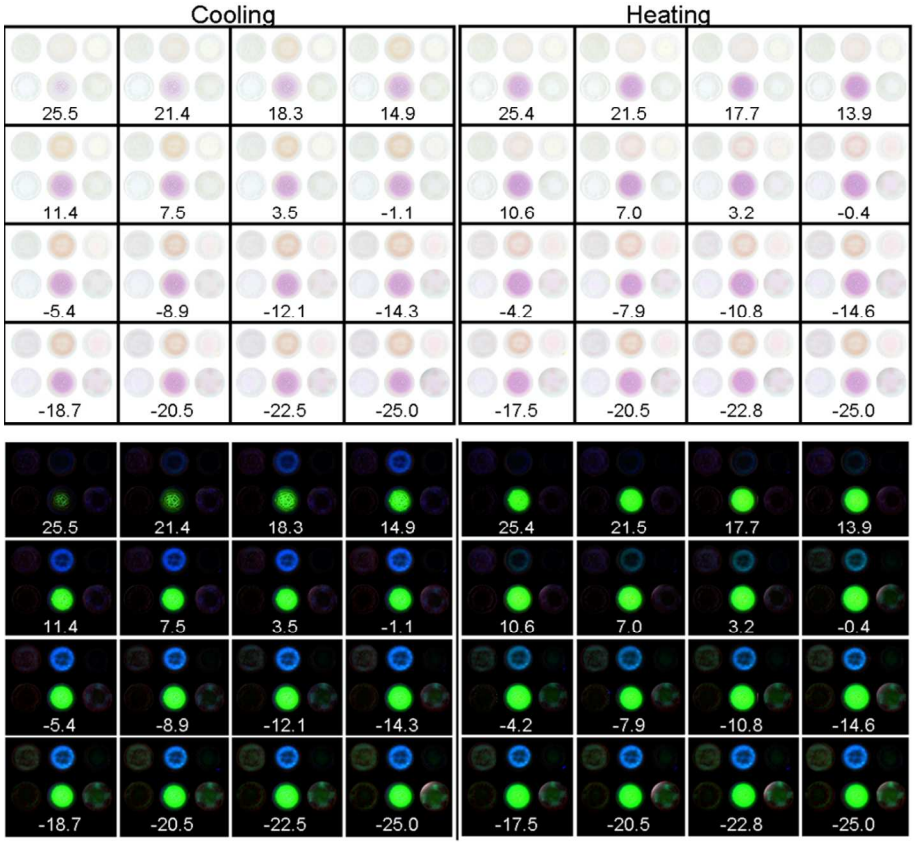

Figure 8. CSA responses to temperature variations in cooling and heating mode. 16 different temperatures are shown in each mode yielding a characteristic colour fingerprint. Below are the corresponding inverted colours of each CSA to clearly define the memory effect based on the colour differences when heating and cooling as well as the fingerprint evolution with temperature.

ANN architecture

As discussed above, the optical behaviour of the SCO/polymer hybrid materials incorporated into the CSA can be fine-tuned depending on the nature of the polymer and the solvent used. The different optical behaviour is in close contact with the midpoint temperatures of the ST hysteresis and the $T_{½}(\downarrow)$. Therefore, based on the colour change of the array, the temperature can be determined readily using a standard chemometric approach using artificial neural networks (ANNs). With this methodology, a non-linear relationship with the temperature can be achieved, overcoming the associated uncertainty with the hysteresis width of each SCO/polymer hybrid material deposited in the films. The goal is to transform a large number of chemical signals into a characteristic temperature response by using both the green channel from RGB and the a* colour coordinate from CIEL*a*b*.

In an attempt to quantify the colour changes, the CSA was digitally imaged and analyzed by standard statistical techniques to extract the average G and a* parameters from RGB and CIEL*a*b* colour spaces, respectively, for all the sensors in the CSA. We obtained the values of these parameters for temperatures ranging from 298.6 to 251.0 K, in five cycles of cooling-heating-cooling-heating-cooling. Then, we discarded the data from cycles 1 to 3 in order to ensure stable sensor data. The remaining values were used as the input to calibrate a Multi-Layer Perceptron (MLP) neural network[41] (see ESI) in charge of predicting the temperature (80% for network training and 20% for network test). The network was trained using the Levenberg-Marquardt algorithm in Matlab R2011a.[42]After the network training, the resulting calibrated MLP was able to estimate the reference temperature with a mean error and standard deviation of 1.25±1.04 K in the calibration data

Model validation

To verify the suitability of the calibration model, we designed an additional experiment to test the new CSA above the temperatures 259.5, 269.1, 281.7 and 294.1 K. The new CSA was applied with heating and cooling cycles over the previous temperatures and we obtained the G and a* parameters from the 6 sensors according to the same procedure explained for calibration, including 6 replicate samples. After that, we removed the two most different samples for each temperature in order to minimize the effect of outliers, and the remaining samples were provided as inputs for the calibrated MLP network to obtain the estimate of their matching temperature.

Table 2. Temperature estimation results in calibration and validation data. The mean error, the standard deviation of the error (S.D), and the maximum error found in the estimation of a sample in the data set are in (ºC);

Data	Mean	S.D.	Max.	R^2	A	B
Calibration	1.25	1.04	3.92	0.99	0.97	$7 \cdot 10^{-17}$
Validation	1.12	0.69	2.73	0.99	1.02	0.03

R^2 is the Determination coefficient; A is the slope of the regression line between reference and predicted temperatures Y=A*X+B while B is the linear coefficient.

Table 2 summarizes the results in both calibration and validation data, including the maximum error in a sample (K), the average error (K) and its standard deviation. The average error is similar in both cases, which suggests that our model was suitably calibrated and can estimate temperatures accurately. In addition, the removal of outliers produced a decrease in both maximum error and standard deviation.

In both models, calibration and validation, the estimated temperatures measured by the sensors were plotted against those coming from the reference device (digital thermometer), expecting a unity slope straight line when fitted by the least-squares (see Table 2).

The regression line was checked simultaneously, where the slope did not differ from the unity and the intercept did not differ from zero (see Table 2). The results obtained show no statistical differences between both sets (calibration vs. reference and validation vs. reference), also corroborating that both calibration and validation models do not have structural errors (see ESI). With these results, we were able to assess the usefulness of the proposed methodology, showing that there are no significant statistical differences between calibration and validation data at a confidence level of 95% (P_{val} of 0.96). Figure 9 shows the regression line between the reference and estimated values while Figure 9.a shows the boxplots for the estimation error distributions in both calibration and validation data sets. Hence, Figure 9 supports the high correlation in the estimated and reference temperatures in both data sets, and the high precision provided by the MLP network.

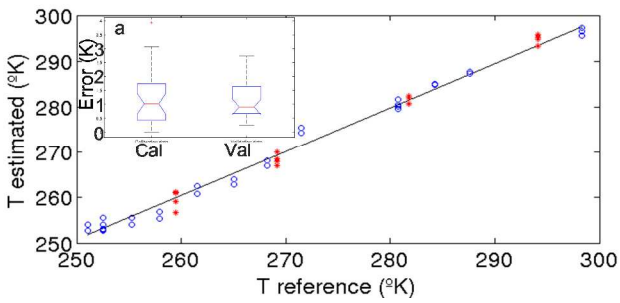

Figure 9. Inset: Boxplots of the error distributions for temperature estimation in calibration and validation data sets against estimated T (K). Regression line between reference (X axis) and predicted (Y axis) temperatures. Blue circles stand for calibration

Conclusions

A disposable CSA for temperature determination was designed by combining an SCO material, $[Fe(NH_2trz)_3](BF_4)_2$, immobilized in six different polymeric matrices and distributed as 3 x 2 thin films. Colour changes related to a spin crossover phenomenon induced by thermal variation make it possible to detect the ST optically. The ST accompanied by thermochromic responses was tracked by a conventional photographic digital camera and by the naked eye. The spin transition of Fe(II), in all films, may be fine-tuned over a wide range by incorporating the SCO material into polymers of an appropriate nature, producing a characteristic thermochromic effect between white colours (HS state), pink, light pink and purple (LS state in the latter three). To identify and assign the structural features in microscopy, a combination between STEM/SEM and microanalysis by EDX were used to verify the expected nanoscale size, in the presence of hydrophilic polymers, and micrometer-sized SCO/polymeric hybrid materials when hydrophobic polymers are used. The SCO particle size in the SCO/polymeric hybrid materials plays an important role in the interaction of the SCO material with the surrounding environment (polymer and solvent molecules). Therefore, a more dense interchain interaction network is expected with hydrophilic polymers, with the LS state becoming predominant at room temperature. This fact was especially observed with the SCO hybrid material in Nafion (with the widest and most pronounced ST) and D6 (less pronounced and shorter ST than in the Nafion/SCO material). The other hybrid materials exhibit a ST displacement to lower temperatures, all showing a loss in the square shape of the hysteresis. For the optical properties, a good linear relationship between the colour of the

SCO/polymer hybrid material with the T½ (↓) and the midpoint temperatures of the hysteresis ST was found. According to the relationship between the colour of the thin films and the ST parameter $T_{½}$ (↓), the following trend is established: Nafion > D6 > $PMMA_{toluene}$ > $PMMA_{THF}$ > PVC_{THF} >PS_{THF}, which is consistent with the proposed influence on the solvent interactions, polymer nature and morphology of the SCO crystals. Thus, there is an obvious relationship between the colours and the ST parameters, which has been successfully matched in this paper. Finally, the CSA has the ability to discriminate temperature between 248 and 298 K, which is useful in food packaging, offering a visual fingerprint of the temperature at which food consumption is best and showing itself to be potentially useful for smart active surfaces.

Experimental Section

Apparatus and Software: A Canon PowerShot G12 digital colour photographic camera with a CCD 1/1.7-inch sensor with 10.0 megapixels (Canon Europe, Amstelveen, The Netherlands) equipped with an 8 GB memory card was used to record colour images. Two ultra bright 4W lamps with 60 LED each (6500k) were used to illuminate the optical sensors (Atmoss Lighting, Alicante, Spain). Adobe Photoshop CS3 Extended ver. 10.0 (Adobe System Inc. San Jose, California, USA) was to obtain the histograms of the images. Later statistical calculations were performed with Excel software (Microsoft, Redmond, WA, USA) and OriginPro v8.0724 (Northampton, MA, USA). A controlled temperature cabinet with a (323 to 223 K) temperature range (refrigerant SUVA HP62 (R-404) A and Zerol ester oil ISO-22) from Revco (Thermo Fisher Scientific Inc. UK) were used. Magnetic measurements were carried out with a Quantum Design (SQUID) magnetometer MPMS-XL-5 with an applied field of 10000 G (0.1 T) with a heating and cooling sweep rate of 10 $K \cdot min^{-1}$. The morphology and the micro elemental analysis of the SCO/polymer hybrid materials were collected by scanning/transmission electron microscopy SEM/STEM using a Zeiss SUPRA40VP equipment operating between 0.2 to 30 kV and coupled with an energy dispersive X-ray (EDX) spectrometer.

Chemicals: To prepare the colourimetric sensor array (CSA), poly(vinylchloride) (PVC; high molecular weight), polystyrene (PS, average MW 280,000, Tg: 100 ºC, GPC grade), poly(methyl methacrylate) (PMMA, average MW 15,000, Tg: 105 ºC, GPC grade), Nafion and tetrahydrofuran (THF) were supplied by Sigma, toluene from Lab-Scan (Dublin, Ireland). A 6 % solution of D6 polyurethane hydrogel (Tyndale Plains-Hunter L.D. Lawrenceville, NJ, USA) in 9:1 ethanol:water mixture was used. The SCO coordination compound $[Fe(NH_2trz)_3](BF_4)_2$ was synthesized according to Kröber et al.[8] Sheets of Mylar-type polyester (Goodfellow, Cambridge, UK) were used as support for the sensor membranes. All the chemicals were of analytical grade and the water used for preparing solutions was purified with a Milli-RO 12 plus Milli-Q water system (Millipore, Bedford, MA).

CSA preparation: On a Mylar support (14 mm x 40 mm x 0.5 mm thick) we prepared an array of 6 test zones (3 x 2) (10 mm in diameter and around 5 µm thick each after solvent evaporation), depositing 25 µL using a dip-coating technique. Once printed, the arrays were aged under nitrogen for at least 5 min before any sensing experiments were performed.

CSA composition: Sensors of different membrane polarities were studied containing 50.0 mg of SCO material $[Fe(NH_2trz)_3](BF_4)_2$ in all cases. The bulk $[Fe(NH_2trz)_3](BF_4)_2$ SCO complex was prepared according to the classical procedure described by Kröber et al.[8] The different mixtures of reagents (cocktails) were: 1) hydrophilic polymer: 6 % solution of D6 in a mixture 9:1 ethanol:water, 2) mixed polarity, hydrophilic-hydrophobic nature: 1 mL Nafion as received, 3) hydrophobic polymers in 1 mL freshly prepared THF as follow: 3.1) 25.0 mg PVC, 3.2) 60.0 mg PS, 3.3) 50.0 mg PMMA and finally 3.4) 50.0 mg PMMA in 1 mL toluene.

Imaging set-up: A constant geometry was maintained with the camera mounted next to a homemade chamber as previously described.[18] The camera parameters were set as follows: the digital camera lens with an aperture (F) 4.5; shutter speed 1/320 seconds; ISO sensitivity 100 and the white balance in the CCD chip setting was maintained constant.

Data analysis: A circular region of interest (ROI) of 200 x 200 pixels from the centre of each sensor was selected. This area was taken to eliminate the influence of artefacts caused by colour variations near the sensor edge, avoiding any sensing film imperfections, uneven responses or vignetting effects.[25] The integration of the circular spot had an average value of 31,416 pixels. Histograms values were between 0 and 255, which corresponds digitally to pure black and white, respectively.

Acknowledgements

The work was funded in part by the Junta de Andalucía, (Spain) (P10-FQM-5974 and P11-FQM-7756), MINECO (CTQ2011-24478), CEI-Biotic CEI-2013-P-2 and Micro-Projects for Young Researchers (CEI-2013-MP-16).

Notes and references

[a] *ECsens Group, Department of Analytical Chemistry, Campus Fuentenueva, University of Granada, 18071 Granada, Spain. Fax: +34 958 243328; Tel: +34 958 248436; E-mail: alejandro_lapresta@hotmail.com*

[b] *Department of Computer Science and Artificial Intelligence, E.T.S. Ingenierías Informática y de Telecomunicación, University of Granada, E-18071 Granada, Spain*

[c] *Departamento de Química Inorgânica. Facultad de Ciencias, Universidad de Granada Avda. Fuentenueva s/n, 18071, Granada, Spain.*

† Electronic Supplementary Information (ESI) available: [Image of the SCO material as bulk and localized EDX analysis for all SCO/polymer hybrid materials.. See DOI: 10.1039/b000000x/

References

1 In *Spin Crossover in Transition Metal Compounds*; Springer: Berlin, 2004.

2 In *Spin-Crossover Materials: Properties and Applications*; John Wiley & Sons: 2013.

3 G. Molnar, L. Salmon, W. Nicolazzi, F. Terki and A. Bousseksou, *J. Mater. Chem. C*, 2014**, 2** (8), 1360-1366.

4 J. Linares, E. Codjovi and Y. Garcia, *Sensors*, 2012**, 12** (4), 4479-4492.

5 C. M. Jureschi, I. Rusu, E. Codjovi, J. Linares, Y. Garcia and A. Rotaru, *Physica B: Condensed. Matter*, 2014**, 449** (0), 47-51.

6 I. Šalitroš, N. T. Madhu, R. Boca, J. Pavlik and M. Ruben, *Monatsh Chem*, 2009**, 140** (7), 695-733.

7 O. Kahn and C. J. Martinez, *Science*, 1998**, 279** (5347), 44-48.

8 J. Kröber, J. P. Audiere, R. Claude, E. Codjovi, O. Kahn, J. G. Haasnoot, F. Groliere, C. Jay and A. Bousseksou, *Chem. Mater.*, 1994**, 6** (8), 1404-1412.

9 L. Salmon, G. Molnar, D. Zitouni, C. Quintero, C. Bergaud, J. C. Micheau and A. Bousseksou, *J. Mater. Chem.*, 2010**, 20** (26), 5499-5503.

10 C. M. Quintero, I. A. Gural'skiy, L. Salmon, G. Molnar, C. Bergaud and A. Bousseksou, *J. Mater. Chem.*, 2012**, 22** (9), 3745-3751.

11 A. Lapresta-Fernández, J. M. García-García, R. París, R. Huertas-Roa, A. Salinas-Castillo, S. Anderson de la Llana, J. F. Huertas-Pérez, N. Guarrotxena, L. F. Capitán-Vallvey and I. Quijada-Garrido, *Part. Part. Syst. Charact.*, 2014**, Accepted** .

12 F. Tanimoto, Y. Kitamura, T. Ono and H. Yoshizawa, *ACS Appl. Mater. Interfaces*, 2010**, 2** (3), 606-610.

13 A. Grosjean, P. Négrier, P. Bordet, C. Etrillard, D. Mondieig, S. Pechev, E. Lebraud, J. F. Létard and P. Guionneau, *Eur. J. Inorg. Chem.*, 2013**, 2013** (5-6), 796-802.

14 Gütlich, P.; Garcia, Y., Chemical Applications of Mössbauer Spectroscopy. In *Mössbauer Spectroscopy*; Yoshida, Y., Langouche, G., Eds.; Springer Berlin Heidelberg: 2013.

15 M. Rubio, R. Herández, A. Nogales, A. Roig and D. López, *European. Polymer Journal*, 2011**, 47** (1), 52-60.

16 H. Winkler, V. Rusanov, J. J. McGarvey, H. Toftlund, A. X. Trautwein and J. A. Wolny, *Hyperfine Interact*, 2006**, 169** (1-3), 1389-1392.

17 A. D. Naik, L. Stappers, J. Snauwaert, J. Fransaer and Y. Garcia, *Small*, 2010**, 6** (24), 2842-2846.

18 A. Lapresta-Fernandez, S. Titos-Padilla, J. M. Herrera, A. Salinas-Castillo, E. Colacio and L. F. Capitan Vallvey, *Chem. Commun.*, 2013**, 49** (3), 288-290.

19 A. Tissot, C. Enachescu and M. L. Boillot, *J. Mater. Chem.*, 2012**, 22** (38), 20451-20457.

20 S. Cobo, G. Molnár, J. A. Real and A. Bousseksou, *Angew. Chem. Int. Ed.*, 2006**, 45** (35), 5786-5789.

21 Y. Chen, J. G. Ma, J. J. Zhang, W. Shi, P. Cheng, D. Z. Liao and S. P. Yan, *Chem. Commun.*, 2010**, 46** (28), 5073-5075.

22 Y. Funasako and T. Mochida, *Chem. Commun.*, 2013**, 49** (41), 4688-4690.

23 M. Clemente-León, E. Coronado, M. López-Jordá, J. C. Waerenborgh, C. Desplanches, H. Wang, J. F. Létard, A. Hauser and A. Tissot, *J. Am. Chem. Soc.*, 2013**, 135** (23), 8655-8667.

24 I. A. Gural'skiy, C. M. Quintero, J. S. Costa, P. Demont, G. Molnar, L. Salmon, H. J. Shepherd and A. Bousseksou, *J. Mater. Chem. C*, 2014**, 2** (16), 2949-2955.

25 A. Lapresta-Fernández and L. Capitán-Vallvey, *Anal. Chim. Acta*, 2011**, 706** , 328-337.

26 A. Lapresta-Fernández and L. F. Capitán-Vallvey, *Analyst*, 2011**, 136** , 3917-3926.

27 Y. Garcia, P. J. van Koningsbruggen, R. Lapouyade, Fournès.Léopold, L. Rabardel, O. Kahn, V. Ksenofontov, G. Levchenko and P. Gütlich, *Chem. Mater.*, 1998**, 10** (9), 2426-2433.

28 O. Kahn, J. Kröber and C. Jay, *Adv. Mater.*, 1992**, 4** (11), 718-728.

29 J. v. Koningsbruggen, Y. Garcia, E. Codjovi, R. Lapouyade, O. Kahn, L. Fournes and L. Rabardel, *J. Mater. Chem.*, 1997**, 7** (10), 2069-2075.

30 A. Tokarev, L. Salmon, Y. Guari, G. Molnar and A. Bousseksou, *New J. Chem.*, 2011**, 35** (10).

31 A. Lapresta-Fernández, A. Salinas-Castillo, S. Anderson de la Llana, J. M. Costa-Fernández, S. Domínguez-Meister, R. Cecchini, L. F. Capitán-Vallvey, M. C. Moreno-Bondi, M.-Pilar Marco, J. C. Sánchez-López and I. S. Anderson, *Critical Reviews in Solid State and Materials Sciences*, 2014**, Accepted** , DOI:10.1080/10408436.2014.899890.

32 Y. Raza, F. Volatron, S. Moldovan, O. Ersen, V. Huc, C. Martini, F. Brisset, A. Gloter, O. Stephan, A. Bousseksou, L. Catala and T. Mallah, *Chem. Commun.*, 2011**, 47** (41), 11501-11503.

33 M. A. Halcrow, *Chem. Soc. Rev.*, 2011**, 40** (7), 4119-4142.

34 K. Schmidt-Rohr and Q. Chen, *Nat. Mater.*, 2008**, 7** (1), 75-83.

35 A. Nakamoto, N. Kojima, L. XiaoJun, Y. Moritomo and A. Nakamura, *Polyhedron*, 2005**, 24** (16–17), 2909-2912.

36 E. M. Levin, Q. Chen and S. L. Bud'ko, *J. Polym. Sci. B Polym. Phys.*, 2012**, 50** (2), 129-138.

37 A. Grosjean, N. Daro, B. Kauffmann, A. Kaiba, J. F. Letard and P. Guionneau, *Chem. Commun.*, 2011**, 47** (45), 12382-12384.

38 S. H. Lim, L. Feng, J. W. Kemling, C. J. Musto and K. S. Suslick, *Nat. Chem.*, 2009**, 1** (7), 562-567.

39 M. C. Janzen, J. B. Ponder, D. P. Bailey, C. K. Ingison and K. S. Suslick, *Anal. Chem.*, 2006**, 78** (11), 3591-3600.

40 C. Zhang and K. S. Suslick, *J. Am. Chem. Soc.*, 2005**, 127** (33), 11548-11549.

41 Haykin, S. In *Neural Networks: A Comprehensive Foundation*; Prentice Hall PTR Upper Saddle River, NJ, USA: 1998; pp 842.

42 M. P. Cuellar, M. Delgado and M. C. Pegalajar, *Proc. Seventh International Conference on Enterprise Information Systems*, 2005**,** 35-42.

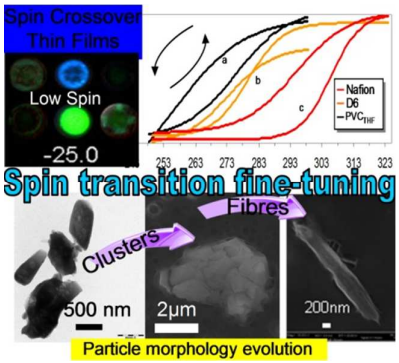

A particle size control of the $Fe(NH_2Trz)_3](BF_4)$ spin crossover material is reached, being its associated thermochromism determined with a photographic digital camera. The hysteretic behaviour is modified to a linear relationship (color vs temperature) by using an ANN design